

2-2-2024

## Meso-structure damage evolution in shear bands of granite residual soil

Cheng-sheng LI

*Department of Civil and Environmental Engineering, Shantou University, Shantou, Guangdong 515000, China; State Key Laboratory of Geomechanics and Geotechnical Engineering, Institute of Rock and Soil Mechanics, Chinese Academy of Sciences, Wuhan, Hubei 430071, China, chengshengli@stu.edu.cn*

Ling-wei KONG

*State Key Laboratory of Geomechanics and Geotechnical Engineering, Institute of Rock and Soil Mechanics, Chinese Academy of Sciences, Wuhan, Hubei 430071, China*

Rong-jun SHU

*State Key Laboratory of Geomechanics and Geotechnical Engineering, Institute of Rock and Soil Mechanics, Chinese Academy of Sciences, Wuhan, Hubei 430071, China*

Zhi-jun LIU

*Department of Civil and Environmental Engineering, Shantou University, Shantou, Guangdong 515000, China*

*See next page for additional authors*

Follow this and additional works at: <https://rocksoilmech.researchcommons.org/journal>



Part of the [Geotechnical Engineering Commons](#)

---

### Recommended Citation

LI, Cheng-sheng; KONG, Ling-wei; SHU, Rong-jun; LIU, Zhi-jun; and ZHANG, Bing-xin (2024) "Meso-structure damage evolution in shear bands of granite residual soil," *Rock and Soil Mechanics*: Vol. 44: Iss. 11, Article 6.

DOI: 10.16285/j.rsm.2022.6732

Available at: <https://rocksoilmech.researchcommons.org/journal/vol44/iss11/6>

This Article is brought to you for free and open access by Rock and Soil Mechanics. It has been accepted for inclusion in Rock and Soil Mechanics by an authorized editor of Rock and Soil Mechanics.

---

## Meso-structure damage evolution in shear bands of granite residual soil

### Abstract

Shear band and crack evolution are very important for landslides. Crack is the weakest area in soil, and there is a lack of effective methods to analyze the meso-structure damage in shear bands quantitatively. To reveal the influence of cracks in granite residual soil on shear deformation and failure, CT scanning was used to obtain volume images of the sample at different loading stages during triaxial loading. Based on the digital volume correlation (DVC) method, a crack classification method is established according to the connectivity characteristics of cracks before and after loading. The cracks can be divided into eight kinds: obsolete, brand-new, isolated, split, combined, compound-brand-new, compound-isolated, and compound-mixed cracks. The results show that the brand-new cracks and compound-type cracks are closely related to the shear band evolution. With the increase of axial strain, the brand-new cracks and compound-brand-new cracks are in an increasing trend. When axial strain is 12%, the volume content of the brand-new cracks is more than 50%, the compound-isolated cracks exhibit rapid attenuation, and the compound-mixed cracks tend to increase first and then decrease. At the early stage of shear band initiation, a few new cracks are formed in the shear band, which accelerates the development of the shear band as the cracks are the weakest area. With the development of the shear band, a large number of new cracks cause more serious damage to the meso-structure in the shear band. Finally, the coupling effect of shear bands and cracks destroys the soil strength.

### Keywords

granite residual soil, CT, shear band, crack classification, damage

### Authors

Cheng-sheng LI, Ling-wei KONG, Rong-jun SHU, Zhi-jun LIU, and Bing-xin ZHANG

## Meso-structure damage evolution in shear bands of granite residual soil

LI Cheng-sheng<sup>1,2</sup>, KONG Ling-wei<sup>2</sup>, SHU Rong-jun<sup>2</sup>, LIU Zhi-jun<sup>1</sup>, ZHANG Bing-xin<sup>1</sup>

1. Department of Civil and Environmental Engineering, Shantou University, Shantou, Guangdong 515000, China

2. State Key Laboratory of Geomechanics and Geotechnical Engineering, Institute of Rock and Soil Mechanics, Chinese Academy of Sciences, Wuhan, Hubei 430071, China

**Abstract:** Shear band and crack evolution are very important for landslides. Crack is the weakest area in soil, and there is a lack of effective methods to analyze the meso-structure damage in shear bands quantitatively. To reveal the influence of cracks in granite residual soil on shear deformation and failure, CT scanning was used to obtain volume images of the sample at different loading stages during triaxial loading. Based on the digital volume correlation (DVC) method, a crack classification method is established according to the connectivity characteristics of cracks before and after loading. The cracks can be divided into eight kinds: obsolete, brand-new, isolated, split, combined, compound-brand-new, compound-isolated, and compound-mixed cracks. The results show that the brand-new cracks and compound-type cracks are closely related to the shear band evolution. With the increase of axial strain, the brand-new cracks and compound-brand-new cracks are in an increasing trend. When axial strain is 12%, the volume content of the brand-new cracks is more than 50%, the compound-isolated cracks exhibit rapid attenuation, and the compound-mixed cracks tend to increase first and then decrease. At the early stage of shear band initiation, a few new cracks are formed in the shear band, which accelerates the development of the shear band as the cracks are the weakest area. With the development of the shear band, a large number of new cracks cause more serious damage to the meso-structure in the shear band. Finally, the coupling effect of shear bands and cracks destroys the soil strength.

**Keywords:** granite residual soil; CT; shear band; crack classification; damage

### 1 Introduction

Granite residual soil is formed by weathering without being transported<sup>[1]</sup> and is widely distributed in the coastal area of southeastern China. Compared to ordinary clay, granite residual soil, as an unusual mixture with better mechanical properties but poorer physical properties in the natural state, contains considerable quartz particles in its fabric. Its mechanical properties are degraded by weathering and complex meso-structures, which makes the soil exhibit significant anisotropy<sup>[3–4]</sup>. This can cause sudden disasters such as slope instability and excavation collapse, posing a serious threat to life and property safety. Most of these engineering problems involve the shear failure behavior of materials, and the current understanding of shear bands and their three-dimensional meso-structure evolution is still insufficient although many studies have been made on macroscopic shear failures of geomaterials.

The initiation, propagation, and connectivity of shear bands are the macroscopical phenomenon of strain localization in the failure process of rock-soil mass<sup>[6]</sup>. The initiation and propagation of shear bands have always been a challenging problem in geotechnical engineering. The connectivity of shear bands is a key factor in soil mass failure, and the change and its characteristics of microstructure are crucial to the evolution of shear bands, as cracks are the weakest areas in soil mass, and the formation of cracks in local

areas may accelerate the connectivity of shear bands.

Among numerous measurement techniques, X-ray computed tomography (CT) scanning has been widely used in the geotechnical field<sup>[7]</sup>. The CT scanning test with real-time triaxial loading was realized for the dynamic analysis of the evolution inside the sample<sup>[8–10]</sup>. It has been proved that CT scanning is powerful in analyzing the meso-structure of materials. For instance, the evolution of crack was qualitatively analyzed based on the three-dimensional (3D) images obtained from the CT scanning<sup>[11–12]</sup>. With the development of image processing technology, pseudo-color information to reflect crack thickness was added to 3D crack visualization<sup>[13]</sup> or pore-size distribution curves were introduced<sup>[11]</sup>. Additionally, graphs of the density change of materials were used to further analyze crack evolution<sup>[14–16]</sup>. These methods are simple and useful but cannot fully exploit the abundant information contained in CT reconstruction. Accordingly, the fractal theory was used to quantitatively characterize 3D crack networks at different loading stages and compare the effects of confining pressure and axial loads on the crack network evolution<sup>[17]</sup>. Cracks generated under external loads in some materials exhibit significant directionality and statistical analyses of the crack density and direction can help to understand the crack evolution<sup>[18]</sup>. The development of the digital volume correlation (DVC) method has allowed its usage to calculate the 3D strain fields of various materials during loading to further analyze the

Received: 3 November 2022

Accepted: 3 January 2023

This work was funded by the Special Fund for Science and Technology of Guangdong Province in 2021 (STKJ2021181), the Building Fund for the Academic Innovation Team of Shantou University (NTF21017) and the National Natural Science Foundation of China (12272394).

First author: LI Cheng-sheng, male, born in 1992, PhD, Lecturer, research interests: soil mechanics of special soils and their macro and meso mechanical properties. E-mail: chengshengli@stu.edu.cn

damage evolution law of materials<sup>[19–20]</sup>. Finite element models can be constructed based on the results of CT reconstruction, and simulation results can be compared with DVC calculation to verify the mesoscopic evolution of cracks<sup>[21]</sup>.

However, there are many pre-existing cracks in granite residual soil<sup>[22]</sup>, and a significant deformation will occur in the sample during triaxial shear. Therefore, it is difficult to use currently available methods to effectively analyze the quantitative evolution law of cracks in shear bands, such as determining which cracks are initiating, obsoleting, or recombining. To analyze the mesoscopic evolution of shear bands in granite residual soil with complex mechanical properties during triaxial shear, the relationship between shear bands and cracks is mainly analyzed in this study. Firstly, the granite residual soil was scanned using CT during triaxial shear testing to obtain volume-rendered images at different loading stages. Then, the 3D strain fields and the shear bands were obtained using the DVC method. Finally, the evolution of the cracks and shear bands was analyzed quantitatively using the improved crack analysis method.

## 2 Experiments and crack analysis methods

### 2.1 Materials and experimental process

The granite residual soil samples were obtained from a foundation pit close to the Houhai subway station in Shenzhen, Guangdong Province. The site from top to bottom concludes Quaternary Holocene Series fill (stone and soil) layer (0–5.7 m), marine sedimentary layer (5.7–7.9 m), Quaternary Holocene alluvial-pluvial deposit layer (7.9–9.3 m), residual soil layer (9.3–20.8 m) and Yanshanian granite (below 20.8 m). The undisturbed cuboidal samples were sampled from the residual soil layer at a depth of 18 m in the pit, protected and packed in a wooden box, and transported back to the laboratory for testing. Table 1 lists the basic physical properties of the samples. It indicates that the granite residual soil possesses a large permeability coefficient, with a high content of coarse and fine quartz particles and a low content of intermediate-sized particles, among which the content of particles with a diameter larger than 0.075 mm exceeds 53%.

**Table 1 Basic physical properties of granite residue soil**

Density $\rho$ /(g · cm <sup>-3</sup> )	Specific gravity $G_s$	Void ratio $e_0$	Water content /%	Coefficient of permeability /(m · s <sup>-1</sup> )	Liquid limit /%	Plastic limit /%	Plasticity index	Gradation (mm) /%			
								>2.000	0.075–2.000	0.005–0.075	<0.005
1.98	2.72	0.74	26.7	$1.79 \times 10^{-6}$	58.89	27.27	31.61	32.4	20.4	18.1	29.1

CT observations were performed using a Vtomex S micron CT scanner comprising an X-ray source, a CT imaging system, and a CT detector. The scanner had a maximum voltage of 240 kV and a maximum resolution of 2  $\mu$ m. The sample was placed on a rotating table controlled by a computer. During the test, the sample and table rotated steadily while the X-ray source stayed still, enabling the 3D scans to be performed (Fig. 1).

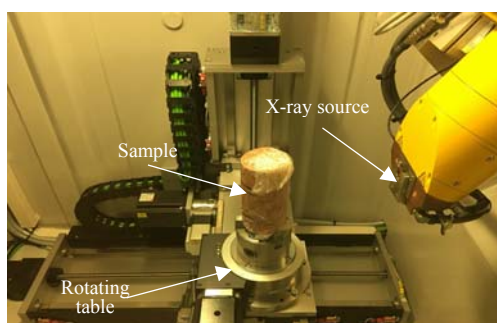


**Fig. 1 Illustration of scanning equipment**

The coarse particles in granite residual soil are relatively large, with the maximum diameter exceeding 5 mm, and the spatial distribution is inhomogeneous. Therefore, the ratio of the maximum particle size to the sample diameter was controlled within 1/10 to make the sample more representative, and the undisturbed samples were cut into cylinders of  $d = 61.8$  mm and  $h = 120$  mm, considering the laboratory

triaxial equipment. Due to the lack of triaxial in-situ CT scanning tests for large-sized samples<sup>[23–25]</sup>, the CT scanning scheme with unloading-step test<sup>[26]</sup> was adopted, with a confining pressure of 200 kPa and a loading rate of 0.12 mm/min for the consolidated undrained (CU) triaxial shear test. As shown in Fig. 2, five groups of CU triaxial tests were carried out with the same confining pressure due to the significant variation in the undisturbed granite residual soil samples, and a representative stress–strain curve was selected as the reference to provide a comparison for the CT triaxial test. The loading process of the CT triaxial test was divided into four steps, with an axial loading increment of 4% each time and a maximum axial strain of 16%. The CT scanning was performed after each loading step, with a total of five scans (including scanning of the samples in the initial state). According to the relationship between the accuracy of the CT scanning equipment and the sample diameter, the CT scanning resolution was set to 38.96  $\mu$ m.

### 2.2 Crack classification method

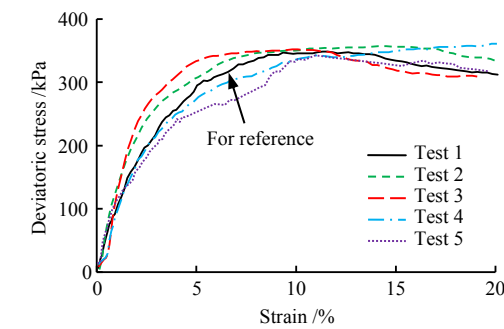
Before the crack evolution analysis, it is necessary to precisely match the 3D spatial positions of the cracks before and after deformation. The particle tracking (particle kinematics) method<sup>[24]</sup> can track the spatial position of particles under different deformations. However, cracks completely differ from hard and stable quartz particles, and their 3D geometry may change, regenerate, or vanish. Thereby, the spatial coordinates of the cracks in the initial stage need to be

accurately transformed to those in the loading stage using the DVC method before the geometric analysis. As illustrated in Fig.3, the cracks are categorized into six types according to their overlapping characteristics before and after deformation [27]:

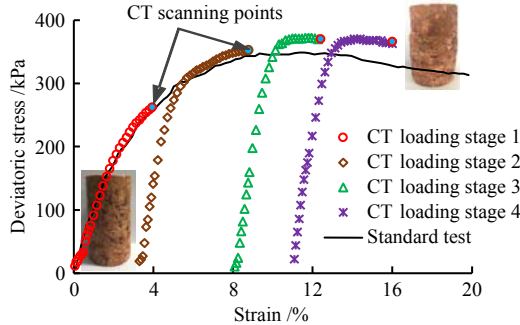
(1) Obsolete cracks. They are observed at the initial stage and do not connect with any other cracks during the loading stage:

$$\forall i, f_i \in \Pi_A \Rightarrow f_i \cap \Pi_B = \emptyset, C_i = 0 \quad (1)$$

where  $C_i$  is the connectivity number of the  $i$ -th crack at the initial stage;  $\Pi_A$  and  $\Pi_B$  represent the cracks sets at the initial stage and the loading stage, respectively;  $f_i$  is the  $i$ -th crack at the initial stage;  $\cap$  represents the crack connectivity calculation.



(a) Curves of parallel triaxial compression tests



(b) Curves of stepwise loading tests and CT scanning points

**Fig. 2 Stress–strain curves and CT scanning points**

(2) Brand-new cracks. They are generated at the loading stage and do not connect with other cracks at the initial stage:

$$\forall j, f_j \in \Pi_B \Rightarrow f_j \cap \Pi_A = \emptyset, C_j = 0 \quad (2)$$

where  $C_j$  denotes the connectivity number of the  $j$ -th crack at the loading stage, and  $f_j$  is the  $j$ -th crack at the loading stage.

(3) Isolated cracks. They have one-to-one connectivity with other cracks at the initial stage:

$$\left. \begin{aligned} \forall \{i, j\}, f_i \in \Pi_A, f_j \in \Pi_B \Rightarrow f_i \cap \Pi_B = f_j, \\ f_j \cap \Pi_A = f_i, C_j = 1 \end{aligned} \right\} \quad (3)$$

(4) Split cracks. They at initial stage connect with the cracks at the multiple loading stages, and the cracks after loading only connect with the cracks at initial stage.

$$\left. \begin{aligned} \forall i, f_i \in \Pi_A \Rightarrow f_i \cap \Pi_B \Rightarrow \{f_{jN}\}, f_{jN} \in \{f_{jN}\} \in \Pi_B, \\ f_{jN} \cap \Pi_A = f_i, C_j = 1, N = 1 \end{aligned} \right\} \quad (4)$$

where  $N$  indicates the number of the  $i$ -th crack at the initial stage that is split into  $N$  cracks, and  $n$  is the subscript of  $N$ , representing the  $n$ -th.

(5) Combined cracks. They at loading stage connect with the multiple cracks at the initial stage, and these cracks at the initial stage only connect with the combined cracks.

$$\left. \begin{aligned} \forall j, f_j \in \Pi_B \Rightarrow f_j \cap \Pi_A = \{f_{iM}\}, f_{iM} \in \{f_{iM}\} \in \Pi_A, \\ f_{iM} \cap \Pi_B = f_j, C_j = 1, M > 1 \end{aligned} \right\} \quad (5)$$

where  $M$  indicates the number of cracks that the  $j$ -th crack at the initial stage is split into  $M$  cracks;  $m$  is the subscript of  $M$ , representing the  $m$ -th.

(6) Compound cracks. The cracks except the above 5 types are compound cracks. This type of crack is complex and exhibits the following characteristics: the crack at the loading stage is connected with the multiple cracks at the initial stage, and those cracks at the initial stage are connected with the multiple cracks at the loading stage.

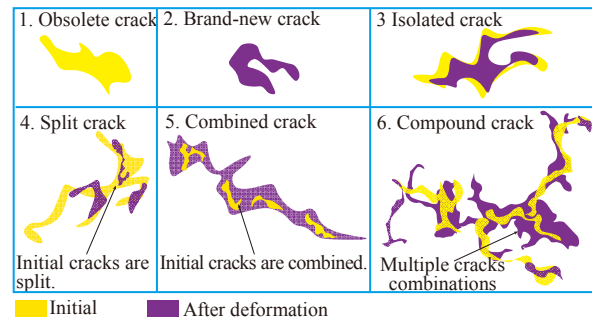


**Fig. 3 Schematic diagram of crack classification method**

According to literature [27], during the shear deformation and failure process of granite residual soil, not only do the brand-new cracks significantly affect the initiation–development–connectivity of shear bands, but also the compound cracks play a key role in the evolution of shear bands. Due to the complex relationship between the initial cracks and the compound cracks, a single index of volume content is not sufficient for an in-depth analysis of the specific effects of compound cracks on shear bands, it is therefore necessary to analyze the compound cracks under the framework of crack classification.

The compound cracks are preliminarily divided into three types according to the 3D spatial overlapping characteristics before and after deformation, as illustrated in Fig. 4:

(1) Compound–brand-new crack (Fig.4(a)): If more than 60% of the total volume of a compound crack does not overlap with the crack at the initial stage, this part is considered as brand new, i.e.:

$$\forall j, f_j \in \Pi_{B,6}, 1 - \frac{V(f_j \cap \Pi_A)}{V(f_j)} \geq 0.6 \quad (6)$$

where  $V$  is the overlapping volume;  $\Pi_{B,6}$  is the compound cracks set at loading stage.

(2) Compound–isolated crack (Fig. 4(b)): If more than 60% of the total volume of the compound crack overlaps with a certain crack at the initial stage, it is considered that this part inherits from the initial crack volume, i.e.

$$\forall \{i, j\}, f_j \in \Pi_{B,6}, f_i \in \Pi_A, \frac{V(f_j \cap f_i)}{V(f_j)} \geq 0.6 \quad (7)$$

(3) Compound–mixed crack (Fig.4(c)): The part that has complex overlapping characteristics, neither being a compound–brand-new crack nor a compound–isolated crack, is defined as a compound–mixed crack.

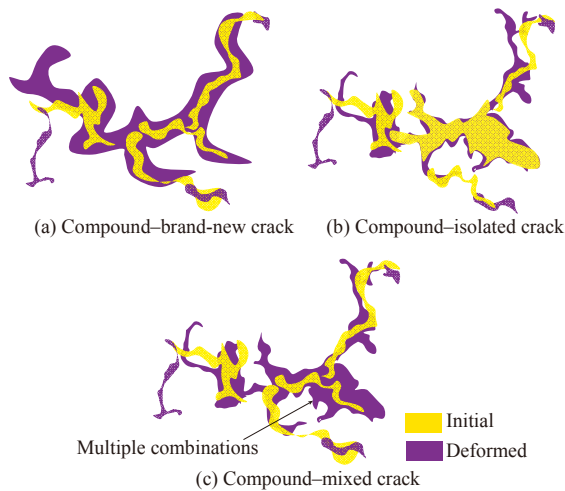


**Fig. 4 Classification diagram of compound cracks**

The proportion of volume overlap of cracks before and after deformation is the basis of the subdivision of compound cracks, and it is set to 60% as a threshold in this paper to represent most of the volume characteristics of the cracks. The geometrical shape of the compound–isolated crack is less affected by the deformation, with at least 60% of the volume unchanged, indicating that the local deformation of the compound–isolated crack is small. On the contrary, over 60% of the volume of the compound–brand-new crack has the properties of “neonatal”, quite different from the initial stage, indicating severe deformation nearby.

$$\bar{\varepsilon} = \sqrt{\frac{2}{9} [(\varepsilon_x - \varepsilon_y)^2 + (\varepsilon_y - \varepsilon_z)^2 + (\varepsilon_z - \varepsilon_x)^2 + 6(\varepsilon_{xy}^2 + \varepsilon_{yz}^2 + \varepsilon_{zx}^2)]} \quad (8)$$

where  $\varepsilon_x, \varepsilon_y, \varepsilon_z, \varepsilon_{xy}, \varepsilon_{yz}, \varepsilon_{zx}$  and  $\varepsilon_{zx}$  are six strain components.

It can be learned from Fig.6 that the overall strain is small and there is no shear band inside the sample under an axial strain of 4%; when the axial strain reaches 8% or more, there is a tilted strain-concentrated region in the middle (a 'V' shape at ¼ profile), and a few local shear bands appear inside the sample. As the axial strain keeps increasing, shear characteristics

### 3 Test result analysis

#### 3.1 Overall crack distribution characteristics

As illustrated in Fig. 5, the calculation domain of the displacement field is defined as an approximate cylinder that is slightly smaller than the diameter of sample to avoid excessive surface deformation of the sample. The sub-volume method was used for DVC calculation, with a grid step of 10 voxels. As mentioned in literature [26], the sub-volume size was 81 voxels × 81 voxels × 81 voxels to achieve optimal matching of digital volume images. This calculation domain can cover most of the sample, including the interest region where shear failure may occur. All of the DVC calculations were implemented by the self-developed iDVC software. (inspire DVC, <https://github.com/lichengsheng HK/iDVC>).

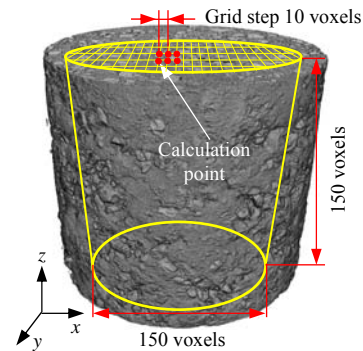


**Fig. 5 DVC calculation parameters**

Figure 6 illustrates the 3D reconstructed volume images and the crack distribution of the granite residual soil at different loading stages obtained using the CT triaxial stepwise loading method, as well as the 3D strain field and the shear bands at four loading stages obtained using the advanced DVC method. Before analyzing the shear bands, the variation pattern of the equivalent strain nephograms was followed, especially the banding characteristics of equivalent strain distribution. As shown in Fig. 6, the 3D strain field presents significant banding characteristics when the equivalent strain exceeds 0.2. Consequently, the part where the equivalent strain exceeds 0.2 is assumed to be a shear band, where the equivalent strain equation is [26]

in the middle of the sample become more evident until significant shear failure occurs, accompanied by a remarkable development of the volume and connectivity of the shear bands. With the further increase of the axial strain, strain localization gradually appears both on the surface and interior as complex 3D bands. As the axial strain progresses, the spatial distribution of shear bands changes from discontinuous initially to connected, and the band thickness gradually increases.

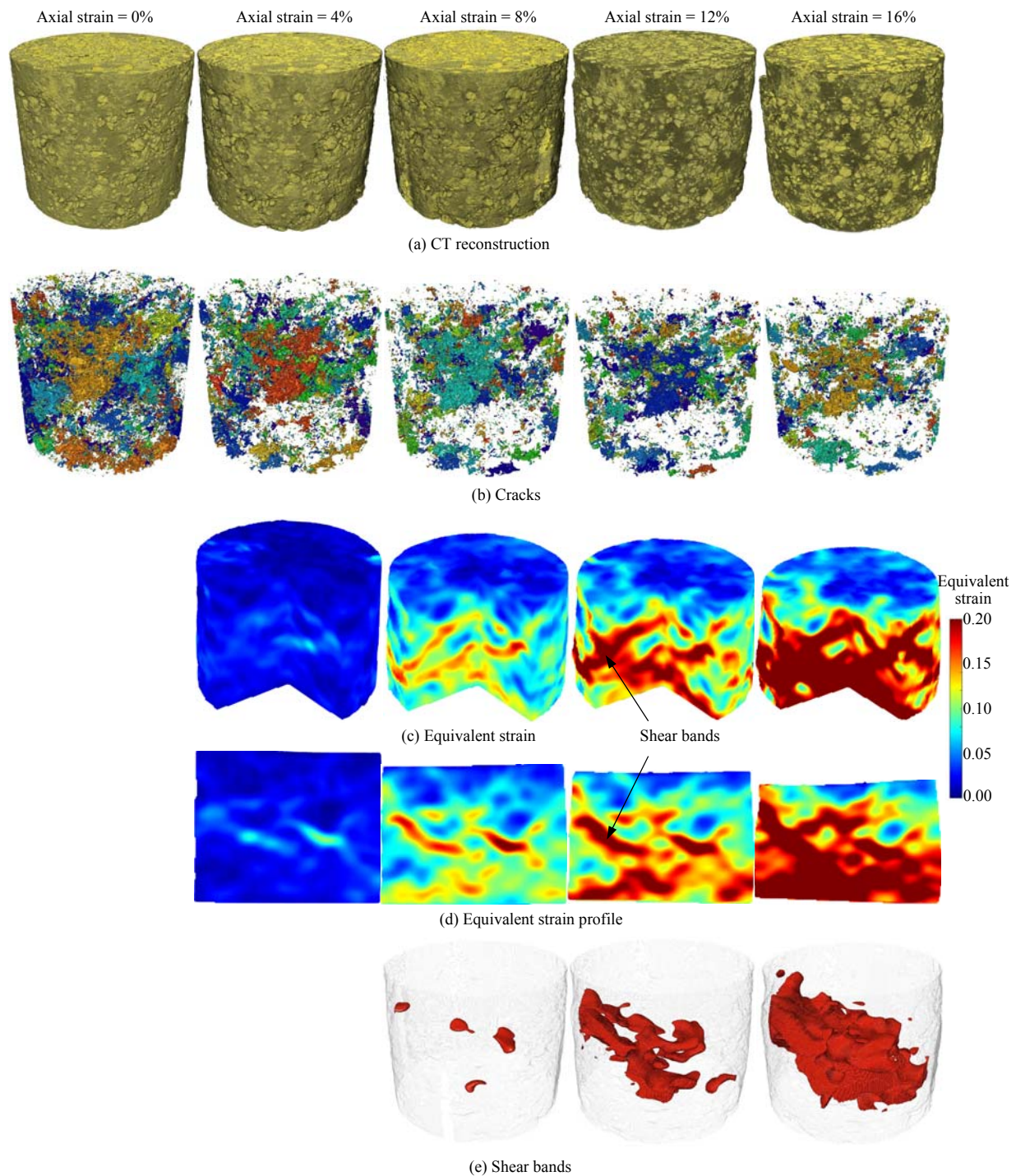


Fig. 6 Volume images, cracks, equivalent strain, and 3D distributions of the shear bands of granite residual soil

The overall volume content of cracks, the volume content of cracks in the shear bands (Fig.7), the content distribution of different types of cracks (Fig. 8), and the pore size distribution of cracks (Fig. 9) have been statistically analyzed to investigate the dynamic evolution law of the cracks inside the sample under loading conditions. The analysis reveals that the volume content of cracks decreases initially and then increases slowly. However, the pore size distribution curves of cracks do not show any noticeable correlation with the triaxial loading stage. As a results, to deeply analyze the dynamic evolution of the cracks during the triaxial shear process, it is important to

accurately classify the cracks.

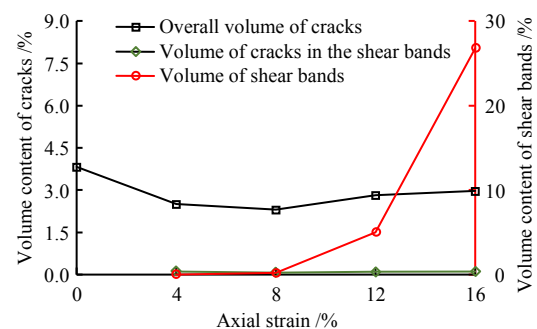
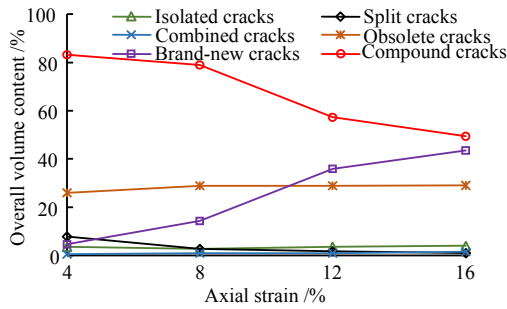
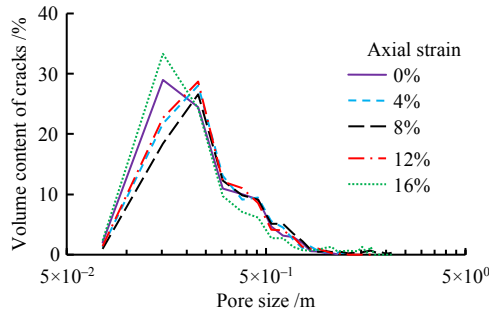


Fig. 7 Volume content of cracks in the sample



**Fig. 8** Volume content curves of different types of cracks in the sample



**Fig. 9** Pore size distribution curves of cracks

Based on the proposed crack classification method, complex 3D cracks are classified into eight categories (Fig.10). It is evident that the volume of compound and brand-new cracks accounts for the largest proportion, with the spatial distribution density of brand-new cracks gradually increasing with the increase of axial strain. Particularly, when the axial strain reaches 12%, a large number of brand-new cracks are generated inside.

Compound cracks undergo complex deformation, with their overall volume gradually decreasing as the axial strain increases:

(1) At the axial strain of 4%, about 80% of the compound cracks were compound–isolated cracks, with

only a few compound–brand-new cracks and compound–mixed cracks, indicating that no significant deformation occurred inside the sample at this stage.

(2) When the axial strain reached 8%, the volume of compound–isolated cracks decreased sharply, while the volume of compound–mixed cracks and compound–brand-new cracks increased rapidly. This point is near the peak of the stress–strain curve shown in Fig. 2. The strain nephogram in Fig. 6 shows that a few shear bands have initiated within the sample, with a large increase of brand-new cracks. This indicates that an intensive deformation has taken place inside the sample, and particularly brand-new cracks have been generated or propagated in the initial cracks. As a result, the volume of compound–mixed cracks has reached its maximum, indicating that the contact relationship of the compound cracks has become more complicated.

(3) With the continuous increase of the axial strain, the volume of the compound–brand-new cracks continues increasing while that of the compound–isolated cracks continues decreasing, and the volume of the compound–mixed cracks follows an increasing-to-decreasing trend.

### 3.2 Evolution of cracks in the shear bands

As shown in Fig. 6 and Fig. 11, when the axial strain is 8%, the dips and dip angles of the shear bands are distributed discretely with no obvious directionality. However, when the axial strain increases to 12%, the shear bands tend to connect and exhibit significant directionality overall, with the dips primarily distributed around 45° and the dip angles ranging from 45° to 58°. At an axial strain of 16%, the number of shear bands grows, and the directionality becomes even more remarkable. Despite the variations in the local characteristics, the failure mode of the shear bands is characterized by the overall inclination.

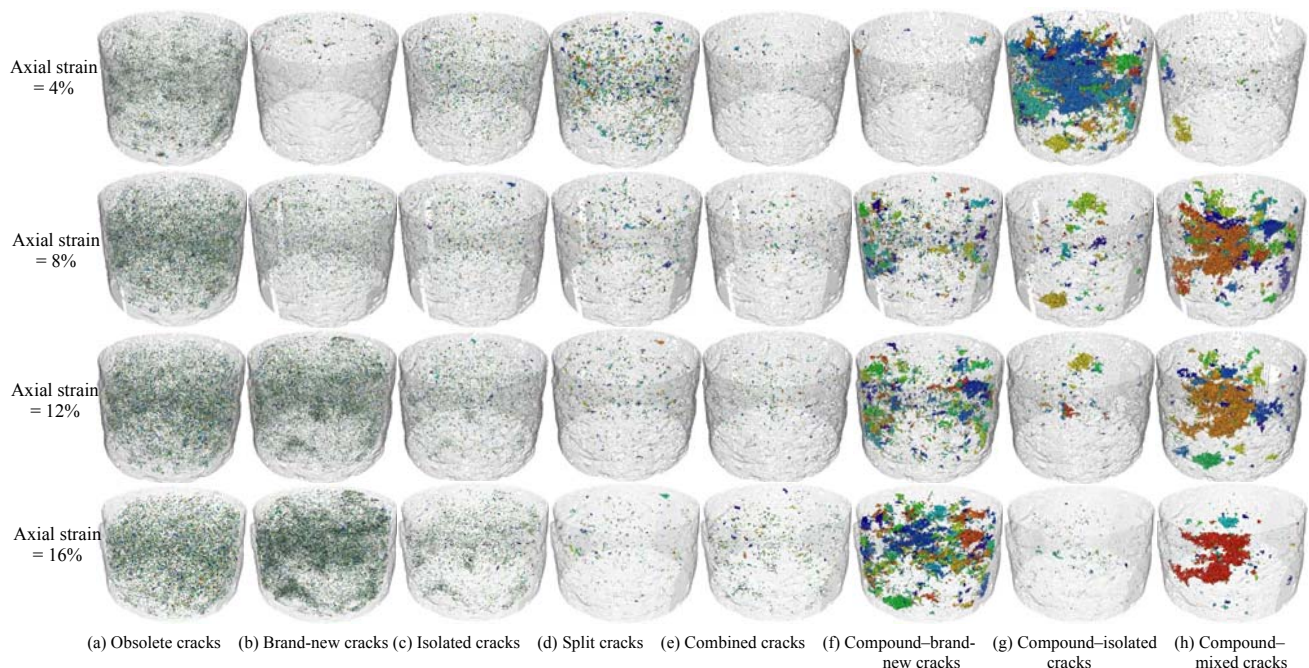


**Fig. 10** Three-dimensional spatial distribution of different types of cracks at different loading stages

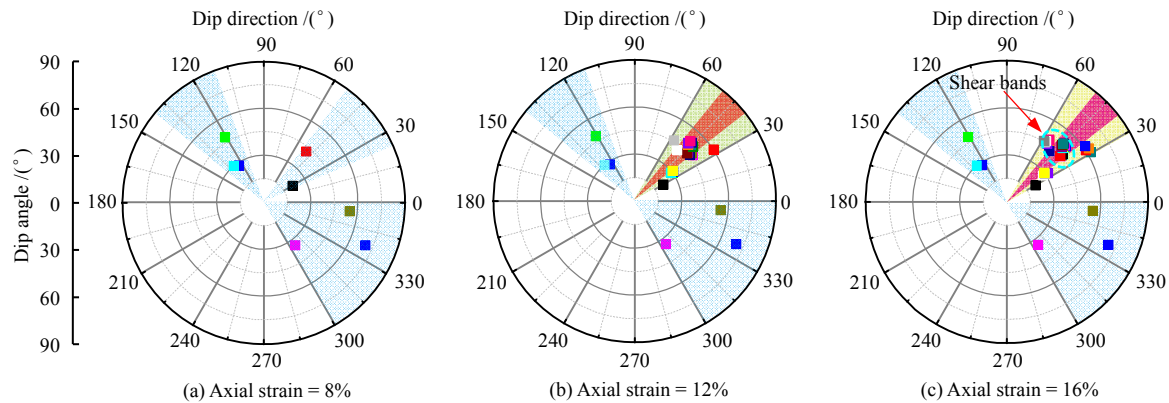


**Fig. 11** Dips and dip angles of shear bands

The deformation and failure of the meso-structure leads to the initiation, propagation, and connectivity of shear bands, and cracks are the weakest area in soils. The triaxial shear failure can be studied by analyzing the overall changes of different types of cracks, but this approach lacks pertinence. This is because the deformation and failure are closely related to the internal strain localization, and cracks are the weakest areas in soils; to quantify which cracks in the initial state have more significant effects on the development of the shear bands, it is necessary to conduct a thorough analysis of the complex cracks to obtain relevant information.

At different loading stages, various shear bands with different connectivities are formed inside the sample, making it difficult to conduct a unified comparative analysis. Therefore, it is necessary to select a representative 3D shear band for inspecting the cracks. The 3D shear band with an axial strain of 12% was selected as a reference according to the evolution and 3D distribution characteristics. Its 3D spatial locations were then transformed to the spatial coordinates at different loading stages, and the statistical analysis of the volume content evolution of different types of cracks in this area was carried out (Fig.7). The cracks play an important role in the evolution of the shear bands, although their volume content is very small, accounting for less than 0.12% of the total volume of the sample and less than 3% of the total volume of the shear band.

Figures 12 and 13 show the distribution and volume contents of different types of cracks in the shear band. The volume contents of brand-new and compound cracks account for the most while those of other types are very small.

With the increase of axial strain, the distribution density of red cracks in the shear band increases gradually, which means the volume of the brand-new

cracks grows gradually with a fast then slow trend. The brand-new cracks tend to grow quickly at the 4%–12% axial strain while the volume content of the corresponding shear band is low, indicating that brand-new cracks play a key role in the initiation and development stage before the connectivity of the shear bands, which has weakened the local strength.

(2) The changes in the compound cracks are complex. The compound–brand-new cracks show a slow increase overall, the compound–isolated cracks show a quick decrease, and the compound–mixed cracks show a quick increase followed by a gradual decrease. As shown in Fig.12, as the axial strain increases, some compound–isolated cracks gradually transform into compound–mixed cracks and finally into compound–brand-new cracks. During the transformation of some compound–isolated cracks into the compound–mixed cracks (axial strain from 4% to 8%), the distribution of the compound cracks reaches the maximum chaos, and the strain is near the critical point of softening on the stress–strain curve. The transformation of partial compound–mixed cracks to compound–brand-new cracks with the increase of the axial strain indicates that the properties of the compound cracks were becoming simpler after the generation of the shear band. Compound cracks generally have large volumes and are analyzed based on the initial cracks, which can effectively reflect the deformation difference of local strain softening.

Studies on brand-new cracks and compound cracks can enhance the understanding of the meso-structure evolution of shear bands and provide a foundation for further in-depth crack-related mechanical analysis, such as evaluating the crack types by combining fracture mechanics and local displacement field characteristics of different cracks. This will help to deeply explore the mechanical characteristics of cracks in the shear bands.

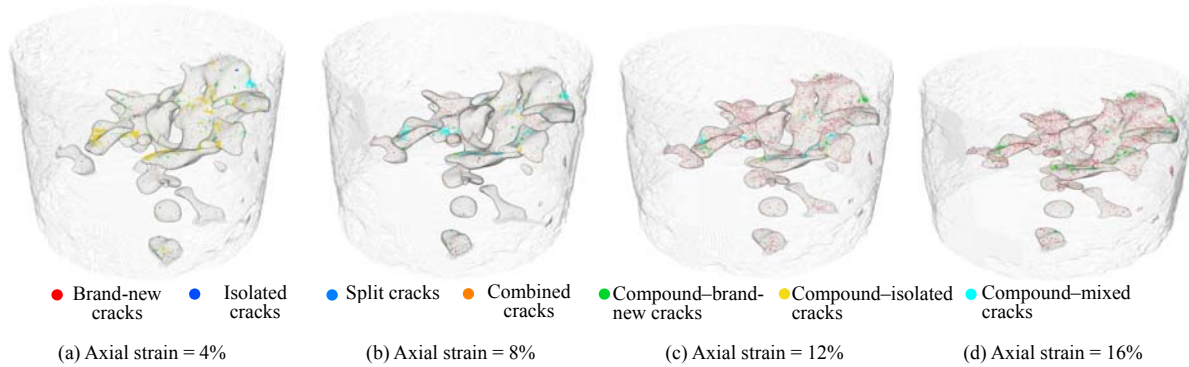
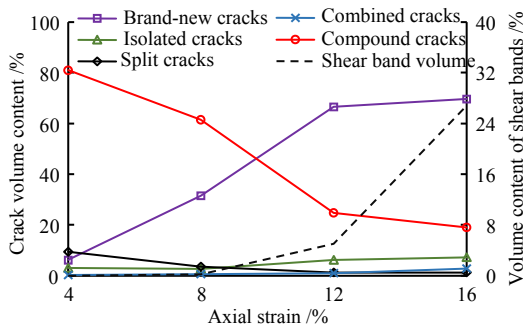
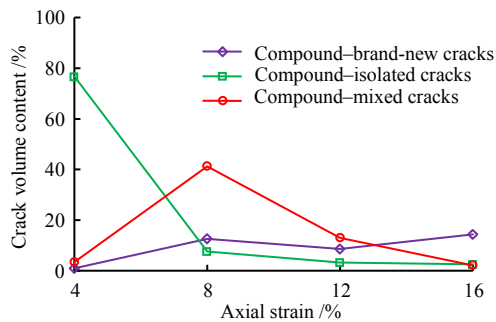


**Fig. 12** Distribution of different types of cracks in the shear bands



(a) Volume of shear bands and evolutions of five types of cracks



(b) Evolutions of three types of compound cracks

**Fig. 13** Volume content evolution curves of different types of cracks in shear bands

## 4 Conclusions

(1) The author developed a refined classification method of compound cracks based on the crack classification method proposed by author and the 3D spatial overlap characteristics of cracks before and after sample deformation. This refined method categorizes compound cracks into the compound-brand-new cracks, the compound-isolated cracks, and the compound-mixed cracks, resulting in eight types of meso-cracks.

(2) The 3D reconstruction details of granite residual soil at different triaxial loading stages obtained by CT scanning were combined with the DVC method and the improved crack classification method proposed in this paper, finding the significant

correlation of the brand-new and the compound cracks with the shear deformation.

(3) The brand new and the compound-brand-new cracks have weakened the local strength and accelerated the development and connectivity of the shear bands inside the sample. The compound-isolated and compound-mixed cracks are both important indicators of the evolution of the shear bands.

(4) The crack classification method proposed is based on CT scanning and the DVC method, and a high CT speckle quality is necessary for the sample to get a high-accuracy 3D displacement field. Therefore, this method is not very applicable to geomaterials such as homogeneous clay and shale.

## References

- [1] WANG Qing, TANG Da-xiong, ZHANG Qing-yun, et al. A study on the structure and composition of granite residual soil in the eastern China[J]. Journal of Changchun University of Earth Science, 1991, (1): 72–81.
- [2] CENG Xiao-ping, ZHOU Qiu-juan, CAI Xiao-ying. Physical properties and shear strength characteristics of high liquid limit granite residual soil[J]. Chinese Journal of Geotechnical Engineering, 2011, 33(6): 901–908.
- [3] BRANCO L P, GOMES A T, CARDOSO A S, et al. Natural variability of shear strength in a granite residual soil from porto[J]. Geotechnical Geological Engineering, 2014, 32(4): 911–922.
- [4] IP C Y S, RAHARDJO H, SATYANAGA A. Spatial variations of air-entry value for residual soils in Singapore[J]. Catena, 2019, 174: 259–268.
- [5] SUN Cheng-wei. Research on granite residual soil engineering properties and subway deep foundation pit design technology[D]. Wuhan: China University of Geosciences, Wuhan, 2014.

- [6] WANG Xue-bin, ZHANG Nan, PAN Yi-shan, et al. Experimental studies of damages and shear band interactions for clay specimens in uniaxial compression[J]. *Rock and Soil Mechanics*, 2018, 39(4): 1168–1175.
- [7] ZHANG Yan-bo, XU Yue-dong, LIU Xiang-xin, et al. Quantitative characterization and mesoscopic study of propagation and evolution of three-dimensional rock fracture based on CT[J]. *Rock and Soil Mechanics*, 2021, 42(10): 2659–2671.
- [8] MAO Ling-tao, YUAN Ze-xun, LIAN Xiu-yun, et al. Measurement of 3D strain field in red stone sample under uniaxial compression with computer tomography and digital volume correlation method[J]. *Chinese Journal of Rock Mechanics and Engineering*, 2015, 34(1): 21–30.
- [9] VAN STAPPEN J, MCBECK J, CORDONNIER B, et al. 4D synchrotron X-ray imaging of grain scale deformation mechanisms in a seismogenic gas reservoir sandstone during axial compaction[J]. *Rock Mechanics and Rock Engineering*, 2022, 55:4697–4715.
- [10] XIN Y, KEMENY J, LI J, et al. 3D observations of fracturing in rock-backfill composite specimens under triaxial loading[J]. *Rock Mechanics and Rock Engineering*, 2021, 54: 6009–6022.
- [11] GEBRENEGUS T, GHEZZEHEI T A, TULLER M. Physicochemical controls on initiation and evolution of desiccation cracks in sand-bentonite mixtures: X-ray CT imaging and stochastic modeling[J]. *Journal of Contaminant Hydrology*, 2011, 126(1-2): 100–112.
- [12] ZAIDI M, AHFIR N-D, ALEM A, et al. Use of X-ray computed tomography for studying the desiccation cracking and self-healing of fine soil during drying-wetting paths[J]. *Engineering Geology*, 2021, 292: 106255.
- [13] SKARYŃSKI Ł, TEJCHMAN J. Experimental investigations of damage evolution in concrete during bending by continuous micro-CT scanning[J]. *Materials Characterization*, 2019, 154: 40–52.
- [14] LOEFFLER C, SUN Q, HEARD W, et al. The effect of loading duration on damage initiation in high-strength concrete[J]. *Mechanics of Materials*, 2019, 140: 103216.
- [15] MAZURIER A, SARDINI P, ROSSI A, et al. Development of a fracture network in crystalline rocks during weathering: study of bishop creek chrono sequence using X-ray computed tomography and 14 C-PMMA impregnation method[J]. *Geological Society of America Bulletin*, 2016, 128: B31336.1.
- [16] TANG C S, ZHU C, LENG T, et al. Three-dimensional characterization of desiccation cracking behavior of compacted clayey soil using X-ray computed tomography[J]. *Engineering Geology*, 2019, 255: 1–10.
- [17] JU Y, XI C, ZHANG Y, et al. Laboratory In situ CT observation of the evolution of 3D fracture networks in coal subjected to confining pressures and axial compressive loads: a novel approach[J]. *Rock Mechanics and Rock Engineering*, 2018, 51(11): 3361–3375.
- [18] WANG Y, QUE J M, WANG C, et al. Three-dimensional observations of meso-structural changes in bimsoil using X-ray computed tomography (CT) under triaxial compression[J]. *Construction and Building Materials*, 2018, 190: 773–786.
- [19] HILD F, BOUTERF A, ROUX S. Damage measurements via DIC[J]. *International Journal of Fracture*, 2015, 191: 77–105.
- [20] LI Ying-jie, ZHANG Liang, WANG Bing-qian, et al. Study on anisotropic three-dimensional deformation field characteristics of shale based on CT scanning and digital volume correlation method[J]. *Rock and Soil Mechanics*, 2023, 44(Suppl.): 134–144.
- [21] YANG Z, REN W, SHARMA R, et al. In-situ X-ray computed tomography characterization of 3D fracture evolution and image-based numerical homogenization of concrete[J]. *Cement and Concrete Composites*, 2017, 75: 74–83.
- [22] LI C, KONG L, GUO A, et al. X-ray microscopic study on disintegration of granite residual soil[Z]. *E3S Web of Conferences*. Glasgow, United kingdom. 2019: 09006.
- [23] ALIKARAMI R, ANDÒ E, GKIOUSAS-KAPNISIS M, et al. Strain localisation and grain breakage in sand under shearing at high mean stress: insights from in situ X-ray tomography[J]. *Acta Geotechnica*, 2014, 10(1): 15–30.
- [24] CHENG Z, WANG J. Quantification of the strain field of sands based on X-ray micro-tomography: a comparison between a grid-based method and a mesh-based method[J]. *Powder Technology*, 2019, 344: 314–334.

- [25] WANG Y, LIU D, HU Y. Monitoring of internal failure evolution in cemented paste backfill under uniaxial deformation using in-situ X-ray computed tomography[J]. *Arabian Journal of Geosciences*, 2019, 12(5): 138.
- [26] LI C, KONG L W, SHU R, et al. Dynamic three-dimensional imaging and digital volume correlation analysis to quantify shear bands in grus[J]. *Mechanics of Materials*, 2020, 151: 103646.
- [27] LI C, KONG L W, AN R. Evolution of cracks in the shear bands of granite residual soil[J]. *Journal of Rock Mechanics and Geotechnical Engineering*, 2022, 14(6): 1956–1966.